



Arabidopsis TBP-ASSOCIATED FACTOR 12 ortholog NOBIRO6 controls root elongation with unfolded protein response cofactor activity

June-Sik Kim^{a,1} , Yuki Sakamoto^{b,c}, Fuminori Takahashi^a , Michitaro Shibata^d , Kaoru Urano^a, Sachihiko Matsunaga^{b,e,f}, Kazuko Yamaguchi-Shinozaki^g, and Kazuo Shinozaki^{a,1}

^aGene Discovery Research Group, RIKEN Center for Sustainable Resource Sciences, Ibaraki 305-0074, Japan; ^bImaging Frontier Center, Research Institute for Science and Technology, Tokyo University of Science, Chiba 278-0022, Japan; ^cDepartment of Biological Sciences, Graduate School of Science, Osaka University, Osaka 560-0043, Japan; ^dCell Function Research Team, RIKEN Center for Sustainable Resource Sciences, Kanagawa 230-0045, Japan; ^eDepartment of Applied Biological Science, Faculty of Science and Technology, Tokyo University of Science, Chiba 278-0022, Japan; ^fDepartment of Integrated Biosciences, Graduate School of Frontier Sciences, The University of Tokyo, Chiba 277-8562, Japan; and ^gResearch Institute for Agricultural and Life Sciences, Tokyo University of Agriculture, Tokyo 156-8502, Japan

This contribution is part of the special series of Inaugural Articles by members of the National Academy of Sciences elected in 2020.

Contributed by Kazuo Shinozaki; received November 5, 2021; accepted December 28, 2021; reviewed by Stephen Howell and Nozomu Koizumi

Plant root growth is indeterminate but continuously responds to environmental changes. We previously reported on the severe root growth defect of a double mutant in *bZIP17* and *bZIP28* (*bz1728*) modulating the unfolded protein response (UPR). To elucidate the mechanism by which *bz1728* seedlings develop a short root, we obtained a series of *bz1728* suppressor mutants, called *nobiro*, for rescued root growth. We focused here on *nobiro6*, which is defective in the general transcription factor component TBP-ASSOCIATED FACTOR 12b (TAF12b). The expression of hundreds of genes, including the *bZIP60*-UPR regulon, was induced in the *bz1728* mutant, but these inductions were markedly attenuated in the *bz1728nobiro6* mutant. In view of this, we assigned transcriptional cofactor activity via physical interaction with *bZIP60* to NOBIRO6/TAF12b. The single *nobiro6/taf12b* mutant also showed an altered sensitivity to endoplasmic reticulum stress for both UPR and root growth responses, demonstrating that NOBIRO6/TAF12b contributes to environment-responsive root growth control through UPR.

unfolded protein response | stress-responsive growth regulation | general transcription factor | root growth

The endoplasmic reticulum (ER) is a eukaryotic organelle where translated peptides undergo protein folding and further modifications before they are secreted as functional proteins. These processes are frequently disturbed by a broad range of intra- and extracellular stimuli that result in the accumulation of malformed proteins inside the ER and cause cellular stress called ER stress. The ER is equipped with a multilayered machinery to cope with such ER stress (1–3). A series of ER-associated protein quality control (ERQC) processes assesses and reprocesses affected proteins to maintain ER homeostasis. In addition, the unfolded protein response (UPR), a dedicated gene-regulatory network, enforces ERQC by inducing the expression of the genes encoding ER-resident chaperones and enzymes in response to ER stress.

UPR is modulated by multiple ER-anchored transcription factors (TFs) and multiple activation pathways. In the model vascular plant *Arabidopsis* (*Arabidopsis thaliana*), the three basic leucine zipper (bZIP) TFs—*bZIP17*, *bZIP28*, and *bZIP60*—are reported to modulate the UPR across the eukaryotes through two different activation pathways (1, 4). *bZIP17* and *bZIP28* are activated by posttranslational activation (5–8); in contrast, *bZIP60* is activated by alternative splicing (9, 10). Whereas studies in mammals have revealed a strong association between the UPR and Alzheimer’s disease and inflammatory diseases (2), plant UPR serves as a versatile stress sensing

mechanism to respond to a wide range of both biotic and abiotic stimuli (1).

The UPR also influences plant growth and development, particularly root growth. We previously reported that an *Arabidopsis* double mutant lacking both *bZIP17* and *bZIP28* function (*bz1728*) displays a severe reduction in vertical root elongation (11). The fact that the loss-of-function of the activator of two bZIPs SITE-2 PROTEASE (S2P) conveyed the similar root growth defects (11, 12), whereas the *bzip17* and *bzip28* single mutants showed normal root growth (5, 6, 11), implies that the UPR controls primary root growth through these two functionally redundant bZIPs. Single *bzip60* mutants or double mutants of *bzip60* and other UPR bZIP genes did not show any growth defects (11). However, the two *bZIP60* activator INOSITOL REQUIRING ENZYME 1A (IRE1A) and IRE1B are reported to modulate primary root growth redundantly with *bZIP17* (13), suggesting that plants employ multiple UPR pathways to various

Significance

Living organisms continuously rebalance their growth and defense/tolerance machineries upon environmental perturbation and energy limitation, which appear as trade-offs. The unfolded protein response (UPR) is a supposed underlying machinery for those trade-offs, responding to a broad spectrum of stress categories and modulating the fundamental growth in both animal and plant systems. We here report the incorporation of general transcription factor NOBIRO6/TAF12b into the UPR-mediated plant root growth control. This indicates that the gene regulation by UPR itself is a key to elucidate the growth trade-offs. Given previously reported roles of NOBIRO6/TAF12b in the signaling of two phytohormones, cytokinin and ethylene, our report proposes how multichannel signals interactively shape plants to survive and thrive in the wild.

Author contributions: J.-S.K., K.Y.-S., and K.S. designed research; J.-S.K., Y.S., F.T., M.S., and K.U. performed research; J.-S.K., Y.S., F.T., and S.M. contributed new reagents/analytic tools; J.-S.K., Y.S., M.S., and S.M. analyzed data; and J.-S.K., K.Y.-S., and K.S. wrote the paper.

Reviewers: S.H., Iowa State University; and N.K., Osaka Prefectural University.

The authors declare no competing interest.

This open access article is distributed under Creative Commons Attribution-NonCommercial-NoDerivatives License 4.0 (CC BY-NC-ND).

¹To whom correspondence may be addressed. Email: june-sik.kim@riken.jp or kazuo.shinozaki@riken.jp.

This article contains supporting information online at <http://www.pnas.org/lookup/suppl/doi:10.1073/pnas.2120219119/-DCSupplemental>.

Published February 3, 2022.

degrees for equivalent root growth control. Clearly, the genetic machinery downstream of the UPR that connects ER stress to root growth is only partially understood.

Here, we describe *Arabidopsis* TATA-BINDING PROTEIN (TBP)-ASSOCIATED FACTOR 12b (TAF12b) as a transcription cofactor mediating UPR-associated root growth control. Eukaryotic transcription initiation starts with the assembly of the transcription preinitiation complex (PIC) onto promoters. The PIC comprises multiple general TF subcomplexes and RNA polymerase II (Pol II). One of these general TFs, TFIID, is a core subcomplex for transcription initiation that consists of TBP and 13 or 14 TAFs, including TAF12. Studies in yeast (*Saccharomyces cerevisiae*) and metazoans revealed that TAF12 functions as a transcription cofactor by physically interacting with other TFs, such as human MYB (14) and activating transcription factor 7 (ATF7) (15), yeast INO5 requiring 2 (Ino2) (16), and repressor/activator site binding protein 1 (Rap1p) (17).

The *Arabidopsis* genome encodes two orthologous copies of TAF12, TAF12a, and TAF12b. A molecular and physiological role was reported for TAF12b from two independent forward genetic studies. TAF12b was first identified as *ENHANCED ETHYLENE RESPONSE 4* (*EER4*) during a screen for mutants exhibiting hypersensitive growth responses to the phytohormone ethylene (18). *EER4* influenced the expression levels of ethylene-responsive genes via its transcriptional cofactor activity and physical interaction with the major ethylene signaling TF ETHYLENE INSENSITIVE 3 (*EIN3*) (18). TAF12b was independently identified as *CYTOKININ-HYPERSENSITIVE 1* (*CKH1*) during a search for mutant callus showing altered responses to another phytohormone, cytokinin (19, 20). The *ckh1* mutant calli were characterized by greening and cellular proliferation due to the deregulation of the cytokinin transcriptional response.

In this study, we aimed to elucidate the mechanism behind the short root phenotype of the *bz1728* double mutant. From a series of reverse and forward genetics approaches, we isolated the *bz1728* suppressor mutant *nobiro6*, which was responsible for partial rescue of root growth. We identified the causal gene, *NOBIRO6*, as encoding TAF12b. We explored the transcriptome landscape of the *nobiro6* single mutant and the *bz1728nobiro6* triple mutant, which revealed that TAF12b acts as a transcriptional cofactor for bZIP60-mediated induction of the UPR. By analyzing the physiological and genetic responses of *nobiro6* single mutants to ER stress, we determined that *NOBIRO6*/TAF12b participates in UPR-associated root growth control and elucidated the molecular mechanism by which TAF12b acts as an important coactivator regulating root growth through the UPR.

Results

As reported previously (11), the 12-d-old *bz1728* seedlings showed a 93.7% reduction in their primary root growth compared to wild-type (WT) seedlings under normal growth conditions (Fig. 1 A and B). To better understand the morphological basis of the short root seen in the *bz1728* mutant, we measured several cell-level growth indices. *Arabidopsis* vertical root growth relies on two major cues: cell division at the root apical meristem (RAM) and longitudinal cell expansion in the elongation zone (EZ), consisting of the cells located shootward from the RAM. We defined RAM size as the longitudinal length from the stem cell niche to the boundary to the EZ in the primary root (Fig. 1C). In 7-d-old *bz1728* seedlings, RAM size decreased by 55.2%, and we scored 55.7% fewer epidermal cells in the RAM compared to WT seedlings (Fig. 1 C–E and *SI Appendix*, Fig. S1). To evaluate the expansion of EZ cells, we measured the longitudinal length of cortical cells in

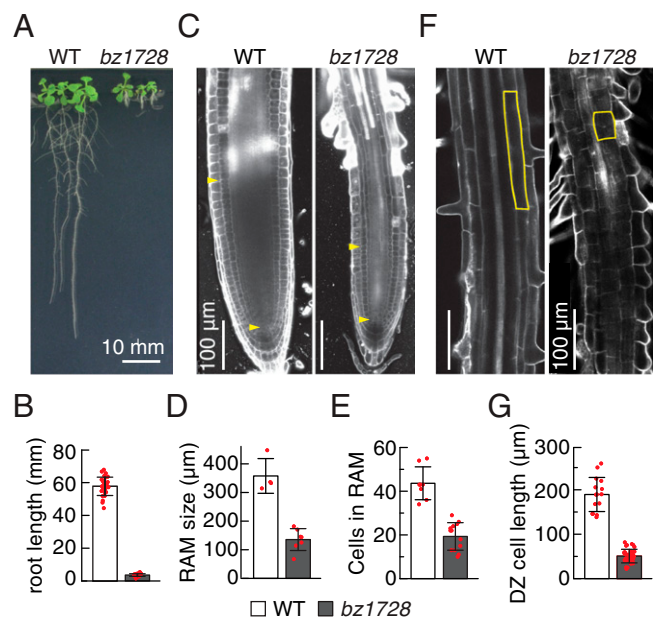


Fig. 1. Characterization of the root growth phenotypes of the *bz1728* double mutant. (A and B) Representative image of 10-d-old vertically grown seedlings (A) and their measured primary root lengths (B). (C–E) Representative magnified view of the RAM from 7-d-old primary roots (C), their measured RAM lengths (D), and the corresponding numbers of RAM cells (E). The RAM area was defined from the stem cell niche (lower yellow arrowhead) to the boundary to the EZ (upper yellow arrowhead) along the primary root (C). (F and G) Representative images of cells in the DZ from 7-d-old primary roots (F) and the measured longitudinal lengths of single DZ cells (G). Representative DZ cells are outlined (F). Data are shown with all data points (red circles) and as bar graphs showing the average \pm SD from at least 10 seedlings (B) or from root cells of three seedlings (D, E, and G). All presented results are significantly different between WT and *bz1728* (Welch's *t* test, $P < 0.001$).

the differentiation zone (DZ), where fully expanded cells undergo terminal differentiation after the EZ. Cells from the *bz1728* mutant elongated 73.2% less than the corresponding WT cells (Fig. 1 F and G). However, we did not observe any visible defect in meristematic cell organization or cell layer differentiation in the root of *bz1728* seedlings. Our cell-level measurements therefore indicated that the short root seen in the *bz1728* mutant is due to compromised growth via combined defects from both RAM activity and longitudinal cell expansion.

Known UPR-Growth Pathways Are Inactive in *bz1728*. The signaling cascade for the phytohormone brassinosteroids (BR) has been reported to be regulated by UPR (12), and several *ems-mutagenized bri1 suppressor* (*eps*) mutations have been shown to suppress the negative UPR effect of BR-mediated vegetative growth (21–23). Accordingly, we generated triple mutants between the *bz1728* double mutant and each of the three *eps* mutants *eps1*, *eps2*, and *eps7*. Root growth was, however, comparable between the *bz1728* mutant and the *bz1728eps* triple mutants (Fig. 2A). We had previously observed that many defense-related genes are spontaneously up-regulated in *bz1728* roots (11). We ectopically expressed the *Pseudomonas putida* gene *NahG* in the *bz1728* mutant background, as *NahG* encodes an enzyme that hydrolyzes the plant defense-signaling phytohormone salicylic acid, thereby weakening defense-related gene expression (24). The resulting transgenic lines displayed noticeably improved shoot growth, but still showed indifferent root growth to *bz1728* (Fig. 2A and B).

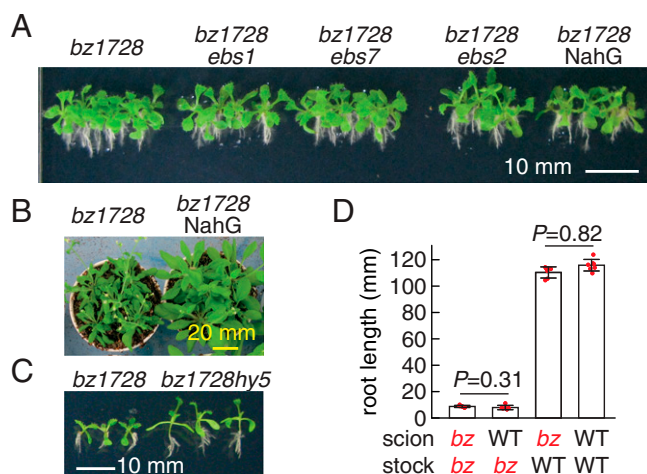


Fig. 2. Reverse genetics approaches to recover the *bz1728* root growth defect. (A) Vertically grown 10-d-old seedlings of *bz1728*, *bz1728ebs* triple mutants (*bz1728* with *ebs1*, *ebs2*, or *ebs7*), and *bz1728* ectopically expressing NahG. (B) Representative image of 26-d-old shoot growth of *bz1728* and *bz1728NahG* plants. (C) Vertically grown 8-d-old seedlings of *bz1728* and the *bz1728hy5* triple mutant. (D) Primary root growth of root-shoot grafted seedlings between WT and *bz1728*. Root growth was measured 7 d after grafting of 3-d-old seedlings. Data are shown with all data points (red circles) and as bar graphs showing the average \pm SD from six biological replicates. Significance coefficient *P* values from Welch's *t* test are provided.

ELONGATED HYPOCOTYL 5 (HY5) is a TF for hypocotyl elongation in response to light and coordinates shoot-to-root signaling for heat-responsive root growth suppression (25). HY5 was also proposed to be a transcriptional repressor of the UPR response by counteracting bZIP28-mediated transcription of UPR-related genes (26). To test the genetic interaction between HY5 and two UPR bZIPs, we crossed a *hy5* T-DNA mutant with the *bz1728* double mutant. The *bz1728hy5* triple mutant had a long hypocotyl and longer petioles, typical of the *hy5* mutant, but the root growth was not affected (Fig. 2C). To further evaluate potential systemic effects of *bz1728* shoots conferred on its short roots, we performed micrografting experiments between the root and shoot tissues of WT and *bz1728* seedlings. Notably, WT shoots did not rescue the growth of mutant rootstocks (Fig. 2D and *SI Appendix*, Fig. S2). We concluded that the root growth defect seen in *bz1728* is independent from any shoot-derived signal, and that previously reported UPR pathways are not involved in the *bz1728* short root phenotype.

The Suppressor Mutant *nobiro6* Partially Rescues the Root Growth of the *bz1728* Mutant. We next conducted a forward genetics screen for suppressors of the *bz1728* short root phenotype. We mutagenized about 20,000 *bz1728* seeds with ethyl methanesulfonate (EMS). We grew M₂ seedlings vertically and selected those with longer roots than their neighbors (Fig. 3A). After validation of the root growth phenotype in subsequent generations, we established a series of unique fertile mutants, which we designated *nobiro* (an imperative verb meaning “to elongate” in Japanese) or *nbr*, suppressor lines.

Of these suppressors, the *bz1728nobiro6* mutant showed a remarkable rescue of root growth. Indeed, primary root growth in the *bz1728nobiro6* mutant rose 478% from that of the *bz1728* mutant in 10-d-old seedlings, reaching 40.8% of WT root length (Fig. 3B). We also analyzed cell-level growth indices in 7-d-old *bz1728nobiro6* seedlings. The reduced RAM size of the *bz1728* mutant returned to WT levels in *bz1728nobiro6* roots. In

addition, the length of cortical DZ cells increased 298% in *bz1728nobiro6* roots relative to those of the *bz1728* mutant, although they only reached 51.9% of the length of the corresponding cells in WT roots (Fig. 3C–F).

Identification of the *nobiro6* Causal Mutation. To identify the causal mutation in *nobiro6*, we generated a backcross population derived from a cross between *bz1728* and *bz1728nobiro6* (*SI Appendix*, Fig. S3). In 10-d-old seedlings, the resulting F₁ progeny had the same root length as the *bz1728* double mutant, while F₂ progeny segregated long roots in a 1:3 ratio (χ^2 test, *P* > 0.89), indicating that *nobiro6* relies on a single recessive mutation. To identify the causal locus, we sequenced the genome of the pooled genomic DNA from 30 F₂ progeny with the *bz1728nobiro6*-type long root, as well as that of three F₂ progeny with a *bz1728*-like short root. By comparison to the *Arabidopsis* reference genome, we identified more than 3,500 single nucleotide mutations for each sequenced sample. We then selected only those mutations that were fixed in the mutant pool and segregating in seedlings with a shoot root, resulting in three nonsynonymous mutations located on the short arm of chromosome 1 (*SI Appendix*, Fig. S3). Of those, one mutation introduced a premature stop codon at residue 431 (Q431X) in a protein-coding gene *At1g17440* (Fig. 3G). This gene became our leading candidate for *NBR6*.

To validate *At1g17440* as *NBR6*, we generated a genome-edited allele of this gene by CRISPR/Cas9 editing (*nbr6-c1*) in the *bz1728* double-mutant background. Sanger sequencing of the *At1g17440* genomic region of the transgenic plant revealed that *nbr6-c1* resulted in a single-nucleotide insertion disrupting the first exon of the gene (Fig. 3G and H). The *bz1728nbr6-c1* line showed the same extent of root growth rescue as *bz1728nobiro6* (Fig. 3I and J). We also produced another triple mutant by crossing a T-DNA insertion line interrupting *At1g17440* (*nbr6-t1*) with *bz1728*; the resulting *bz1728nbr6-t1* seedlings showed a rescue of root growth similar to that seen in *bz1728nobiro6* seedlings (Fig. 3G, I, and J). Together, these results confirmed that *At1g17440* is *NBR6* and that all three mutant alleles (*nobiro6*, *nbr6-c1*, and *nbr6-t1*) are equivalently strong loss-of-function alleles that partially rescue the root growth defect characteristic of the *bz1728* double mutant.

The *nbr6* Mutation Decreased the Transcription of *bz1728*-Induced Genes. *NBR6* encodes TAF12b, one of the two *Arabidopsis* orthologs of eukaryotic TAF12 and a subunit of the general TF TFIID. Since previous studies identified *NBR6* as a novel transcription cofactor in phytohormone signaling (18, 20), we anticipated that the *nbr6* mutation might modulate the transcriptome of the *bz1728* mutation to exert its visible rescue of root growth.

To explore this possibility, we performed transcriptome deep sequencing (RNA-seq) on root samples collected from 12-d-old WT, *bz1728*, *bz1728nobiro6*, and the single *nbr6-t1* mutant seedlings. We identified differentially expressed genes (DEGs) in each mutant in comparison to the WT with a |fold-change (FC)| \geq 2 and a false-discovery rate < 0.05. We obtained more than 2,000 DEGs in the *bz1728* double mutant; they presented roughly equal distribution between down-regulated and up-regulated genes (Fig. 4A). Although we identified the same number of DEGs in the *bz1728nobiro6* triple mutant, more DEGs were down-regulated and fewer DEGs were up-regulated relative to the double mutant. Indeed, the mean FC of down-regulated DEGs decreased from 9.48 to 6.50 (Fig. 4A). Of the top 200 up-regulated DEGs in the *bz1728* double mutant, only 46 were differentially expressed in the *bz1728nobiro6* mutant; in contrast, of the top 200 down-regulated DEGs in the *bz1728* double mutant, 166 remained differentially expressed in the *bz1728nobiro6* triple mutant (Fig. 4B). The transcriptional effects of the single *nbr6-t1* mutant were much

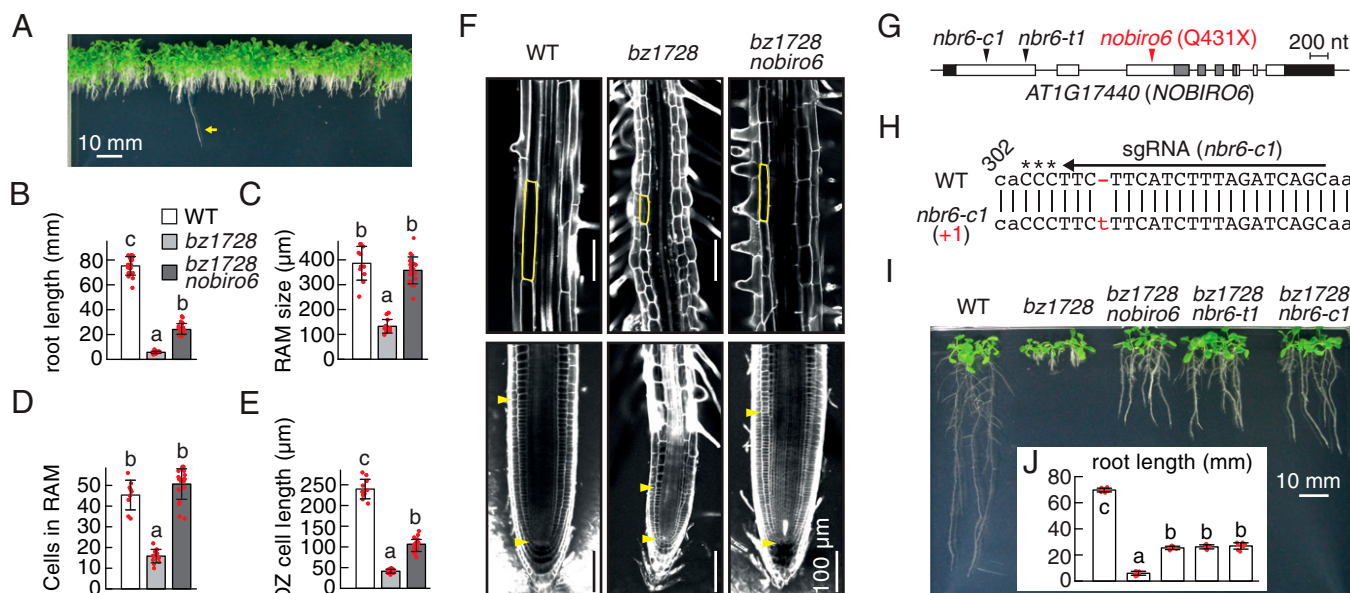


Fig. 3. Identification of the *bz1728* suppressor mutant *nobiro6*. (A) Vertically grown 10-d-old *nobiro* M₂ seedlings of mutagenized *bz1728*. The yellow arrow indicates the *bz1728nobiro6* seedling. (B–F) Characterization of root growth in 7-d-old *bz1728nobiro6* seedlings. Primary root growth (B), number of RAM cells (C), longitudinal length of the RAM (D), longitudinal length of DZ cells (E), and representative views around the DZ (Upper) and the RAM (Lower) are presented (F) from WT, *bz1728* and *bz1728nobiro6* seedlings. The RAM area was defined from the stem cell niche (lower arrowhead) to the boundary to the EZ (upper arrowhead) along the primary root. (G) Identification of *NOBIRO6*. White and gray boxes, exons; black lines, introns; black boxes, untranslated regions; gray boxes, eukaryote-conserved HFD. Red arrowhead, EMS-induced *nobiro6* allele; black arrowheads, position of the T-DNA insertion (*nbr6-t1*) and genome-edited site (*nbr6-c1*). (H) Genotype of the CRISPR/Cas9-mediated genome-edited allele *nbr6-c1*. (I and J) Representative image of vertically grown 10-d-old seedlings of WT, *bz1728*, *bz1728nobiro6*, and two *bz1728nbr6* mutants (I) and their primary root growth (J). Data are shown with all data points (red circles) and as bar graphs showing the average \pm SD from more than 10 seedlings (B), from root cells of three seedlings (C–E), or from six biological replicates (J). Different letters indicate significant differences (ANOVA post hoc Tukey's HSD test, $P < 0.01$).

more subtle, supporting a subsidiary cofactor role for NBR6 in global gene regulation (Fig. 4A). Previous studies on NBR6/TAF12b reported dozens of genes whose expression were affected in its single mutants with names of *eer4* (18) or *ckh1* (20). We therefore assessed these gene-expression patterns in the single *nbr6-t1* mutant and observed changes in line with those described for *eer4* but not for *ckh1* (SI Appendix, Table S1). The apparent discrepancy concerning *ckh1* might reflect the different tissues analyzed: differentiated tissues (*eer4* and *nbr6-t1*) and dedifferentiated calli (*ckh1*). Our RNA-seq analysis thus revealed that the rescue of the limited root growth seen in the *bz1728nobiro6* mutant is accompanied by a suppression of transcriptional up-regulation dynamics in the *bz1728* short root.

NBR6 Physically Interacts with the UPR TF bZIP60. bZIP60 is another transcriptional activator that modulates the UPR together with bZIP17 and bZIP28; we previously reported its spontaneous overactivation in the *bz1728* mutant (11). We therefore determined the expression pattern of the regulon consisting of bZIP60 target genes with additional *nbr6* mutation. Indeed, the expression of most genes from the bZIP60 regulon was highly induced in the *bz1728* mutant relative to WT, but diminished in the *bz1728nobiro6* triple mutant (SI Appendix, Table S2). We confirmed the relative transcript levels of bZIP60 and two of its representative target genes, *SECRETORY 31A* (*SEC31A*) and *BINDING PROTEIN 3* (*BIP3*), in *bz1728* and *bz1728nobiro6* seedlings by qRT-PCR (Fig. 4C). We therefore hypothesized that NBR6 functions as a transcriptional coactivator of the bZIP60 regulon.

A role in transcriptional regulation would require that NBR6 localize to the nucleus, and it has been revealed by previous reports (18, 20). For further molecular details, we tested the subcellular localization of NBR6 and various truncated versions as fusion proteins with superfolder green fluorescent

protein (sGFP). NBR6 is a 684-aa protein with a single histone-fold domain (HFD) at its C terminus and multiple unannotated glutamine-rich repeats in its N-terminal long tail. We transiently transfected *Arabidopsis* protoplasts with constructs encoding full-length sGFP-NBR6f, the N terminus of NBR6 without the HFD (amino acids 1 to 502; sGFP-NBR6n) or the NBR6 C terminus including the HFD (amino acids 496 to 684; sGFP-NBR6c) (Fig. 4D). Both sGFP-NBR6f and sGFP-NBR6c localized to the nucleus, whereas sGFP-NBR6n accumulated throughout the cell (Fig. 4E). These observations indicated that the nucleus localization of NBR6 depends on the HFD within its C terminus.

We then assessed the physical association of NBR6 and its derivatives with bZIP60 by bimolecular fluorescence complementation (BiFC) assay by transient transfection of *Arabidopsis* protoplasts (27). A C-terminally truncated form of bZIP60 (bZIP60n) was employed for its spontaneous nuclear localization (28). We observed reconstitution of yellow fluorescent protein (YFP) for all combinations of transfected constructs expressing bZIP60n-YFP^C and NBR6f-YFP^N, NBR6n-YFP^N, or NBR6c-YFP^N, with a strong overlap between YFP fluorescence and that obtained for the nucleus marker histone H2B fused to cyan fluorescent protein (CFP) (Fig. 4F). As an independent confirmation, we conducted a split-luciferase complementation (split-LUC) assay by transient infiltration of *Nicotiana benthamiana* leaves (29). Consistent with the BiFC results, we detected LUC activity for all combinations of constructs, but not for individual constructs (Fig. 4G). These results supported the physical interaction of NBR6 and bZIP60 in the nucleus. However, how both NBR6c and NBR6n can functionally interact with bZIP60 was not clear.

We hypothesized that NBR6 interacts with bZIP60 only via a single domain, whereas NBR6n can indirectly interact with bZIP60 through the larger TFIID complex. To test this

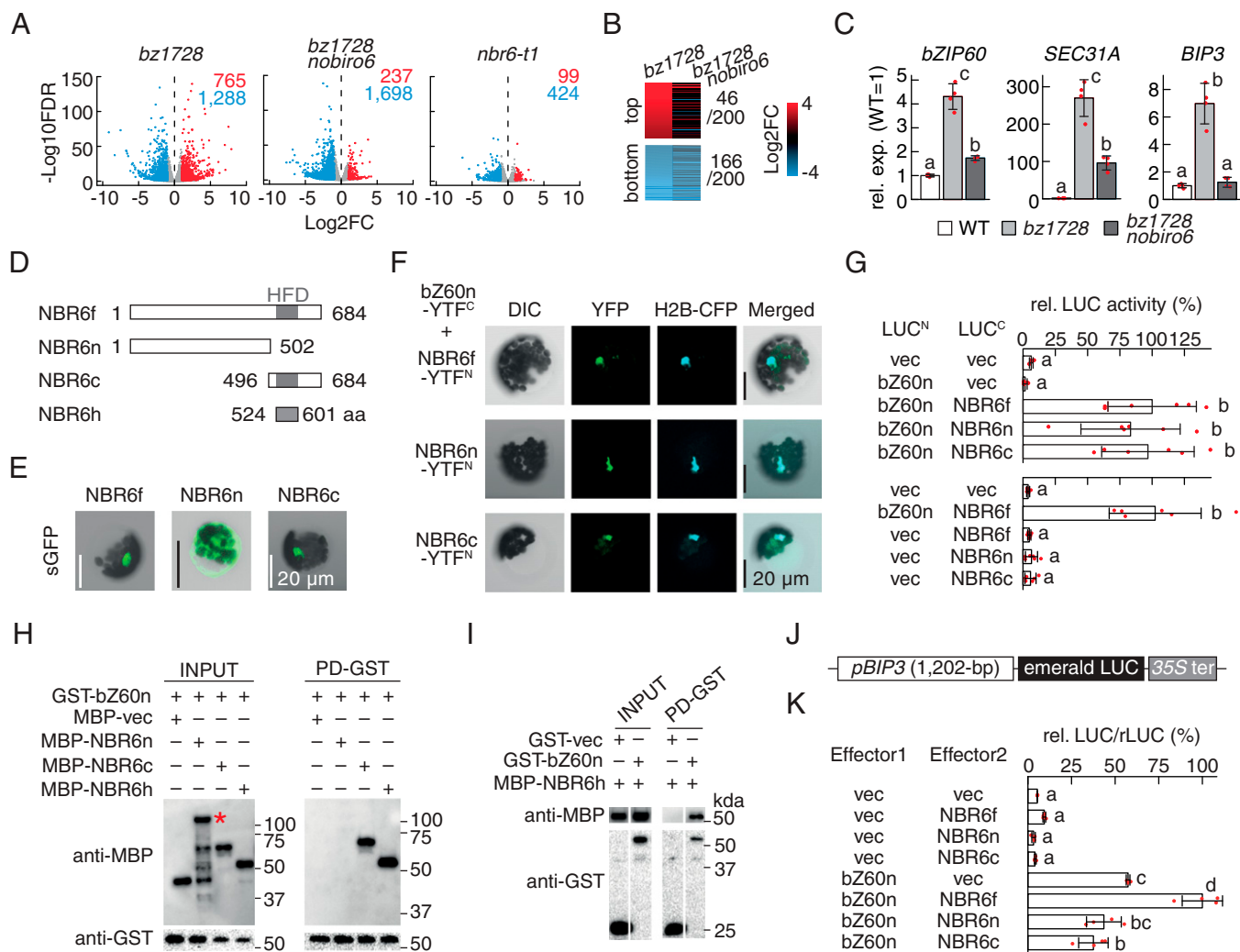


Fig. 4. Transcription cofactor activity of NBR6. (A) Volcano plots illustrating the transcriptome dynamics in double *bz1728*, triple *bz1728nobiro6*, or single *nbr6-t1* mutant in 12-d-old roots. (B) Heatmap representation of FC (\log_2FC) for the top 200 most up-regulated or down-regulated genes in *bz1728* and *bz1728nobiro6*. (C) Relative transcript levels for representative UPR-related genes under normal growth conditions, as determined by qRT-PCR. Values in WT were set to 1. (D) Schematic diagram of NBR6 and derivatives used in this study. Gray box indicates the eukaryote-conserved HFD. (E) Fluorescence signal observed in *Arabidopsis* protoplasts transiently transfected with constructs encoding sGFP-tagged NBR6 derivatives. (F) BiFC signal observed for combinations of constructs encoding C-terminally truncated bZIP60 (bZ60n) and NBR6 derivatives. Constructs were transiently transfected in *Arabidopsis* protoplasts. DIC, differential interference contrast; H2B-CFP, CFP fluorescence as transfection control and nuclear localization marker; merged, merged image; YFP, YFP fluorescence by BiFC. (G) Split-luciferase complementation (split-luc) signal observed from combinations of constructs encoding bZ60n and NBR6 derivatives. Constructs were transiently infiltrated in *N. benthamiana* leaves. (H and I) In vitro pull-down assays between GST-bZ60n and MBP-NBR6 derivatives. Representative immunoblot results of input samples (INPUT) and pulled-down samples with anti-GST antibody (PD-GST) are shown. The asterisk indicates the expected band size for MBP-NBR6n. (J and K) Transient transactivation assay for bZ60n and NBR6 derivatives. The schematic diagram of the reporter construct with the *BIP3* promoter is shown (J). Data are shown with all data points (red circles) and as bar graphs showing the average \pm SD from four (C and K) or six (G) biological replicates. Different letters indicate significant difference (ANOVA post hoc Tukey's HSD test, $P < 0.01$). vec, blank vector control.

hypothesis, we performed a pull-down assay using protein extracts and partially purified recombinant proteins from TFIID-free *Escherichia coli*. Accordingly, we purified recombinant glutathione S-transferase (GST)-bZIP60n and mixed the protein with lysates from cells induced to accumulate maltose-binding protein (MBP)-NBR6 and derivatives (SI Appendix, Fig. S4). After pull-down with anti-GST antibody, we detected MBP-NBR6c, but not MBP-NBR6n or MBP, in the precipitates (Fig. 4H). The HFD (amino acids 524 to 601; NBR6h) was also pulled down by GST-bZIP60 when fused to MBP (Fig. 4D, H, and I and SI Appendix, Fig. S4). We concluded that NBR6 physically interacts with bZIP60 through the HFD in the nucleus.

Having established their physical interaction, we next evaluated the transcriptional cofactor activity of NBR6 toward bZIP60, via transient transfection in *Arabidopsis* mesophyll protoplasts. We

used the *BIP3* promoter (*pBIP3*) driving the transcription of the emerald firefly luciferase (*eLUC*) reporter gene as the target of bZIP60, as previously reported (28). Transient transfection of *bZIP60n* alone induced eLUC activity from the *pBIP3:eLUC* reporter more than 10-fold over empty vector controls, but cotransfection of *bZIP60n* and full-length *NBR6* raised eLUC activity another 1.85-fold (Fig. 4J and K). The cotransfection of *bZIP60n* and *NBR6n* or *NBR6c* failed to enhance the transactivation mediated by bZIP60n (Fig. 4K). Together, these results demonstrate that NBR6 functions as a transcriptional cofactor to bZIP60 via physical interaction through its HFD in the nucleus.

The *nbr6* Mutation Alleviates the ER Stress-Induced Root Growth Reduction. We next wished to determine to what extent the loss of NBR6 alone might affect plant responses to ER stress.

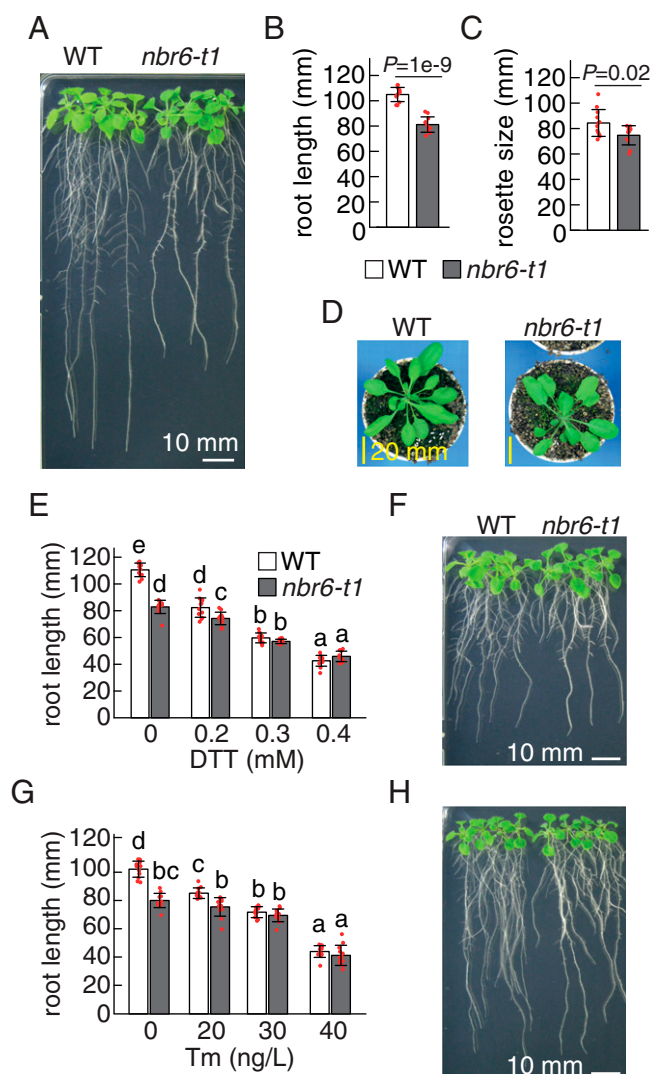


Fig. 5. Root growth response to ER stress of *nbr6-t1* single mutant. (A–D) Root and shoot growth of the *nbr6-t1* single mutant. Representative image of vertically grown 12-d-old seedlings (A) and their primary root growth (B). Diameter of 28-d-old rosettes (C) and representative images (D). (E–H) Root growth in response to ER stress. (E and G) Primary root growth was measured 7 d after transferring 3-d-old seedlings to various concentrations of the ER stress inducers DTT (E) or Tm (G). (F and H) Representative images of root growth under 0.3 mM DTT (F) or 30 ng L⁻¹ Tm (H). Data are shown with all data points (red circles) and as bar graphs showing the average \pm SD from six (B and C) or eight (E and G) biological replicates. Significance coefficient *P* values from Welch's *t* test are provided (B and C). Different letters indicate significant difference (ANOVA post hoc Tukey's HSD test, $P < 0.01$) (E and G).

Under normal growth conditions, the *nbr6-t1* single mutant showed a mild reduction in the growth of both roots and shoots. The length of the primary root from 12-d-old *nbr6-t1* seedlings was 87.3% that of WT (Fig. 5 A and B). Similarly, rosette diameter of 28-d-old *nbr6-t1* plants was 11.5% smaller than that in WT plants of the same age (Fig. 5 C and D).

To further characterize the phenotypes of *nbr6* single mutants, we measured root growth upon activation of ER stress. Accordingly, we transferred 2-d-old seedlings grown on normal growth medium to fresh medium containing various concentrations of the two ER stress agents, tunicamycin (Tm) and dithiothreitol (DTT). After 10 d on the new medium, primary root elongation in WT seedlings had decreased in a dose-dependent

manner for both Tm and DTT, as previously reported (26, 30, 31) (Fig. 5 E and G). Although primary root growth also slowed down in the *nbr6-t1* single mutant as an effect of the ER stress agent, the mutant response was less pronounced than that of WT seedlings, as *nbr6-t1* roots were already shorter than WT under control conditions and failed to respond to higher concentrations of Tm and DTT (Fig. 5 E–H). We interpret these results as indicating the possible participation of NBR6 to ER stress-responsive control of root growth.

The *nbr6* Mutation Alters UPR Activity. To investigate stress-responsive UPR activity in the *nbr6-t1* mutant, we collected root tissues from seedlings grown on 30 ng L⁻¹ Tm (Fig. 5F) to measure relative transcript levels of the representative UPR target genes *BIP3* (a shared target of bZIP28 and bZIP60), *SEC31A* (a bZIP60 target), and *CALRETICULIN 2* (*CRT2*, a bZIP28 target) by qRT-PCR (11, 32, 33). Tm induced the expression of all three genes in WT, as expected (Fig. 6A). Importantly, relative transcript levels reached lower levels in the *nbr6-t1* mutant. In addition, all three genes were slightly induced even under control conditions in the mutant, resulting in a 40 to 50% reduction in their FC between control and Tm treatment (Fig. 6B). This result was consistent with the alleviation of root growth reduction upon ER stress in the *nbr6-t1* mutant (Fig. 5 E–H).

To obtain a global view of the apparent induction of the UPR by the *nbr6-t1* mutant under control conditions, we looked at the transcript levels of other UPR-related genes in our RNA-seq dataset (Fig. 4A). In addition to *BIP3*, *SEC31A*, and *CRT2*, we determined transcript levels for 20 known UPR target genes and three UPR-bZIP genes in WT and *nbr6-t1*. We grouped UPR target genes into three clades based on the bZIP regulating their transcription, bZIP28 targets, bZIP60 targets, and bZIP28 and bZIP60 shared targets, as reported previously (11). The transcript levels of all three bZIP genes and most of their target genes increased in the *nbr6-t1* mutant (Fig. 6C). Notably, the transcription of bZIP28 and bZIP60 shared target genes was more weakly induced than that of the other clades.

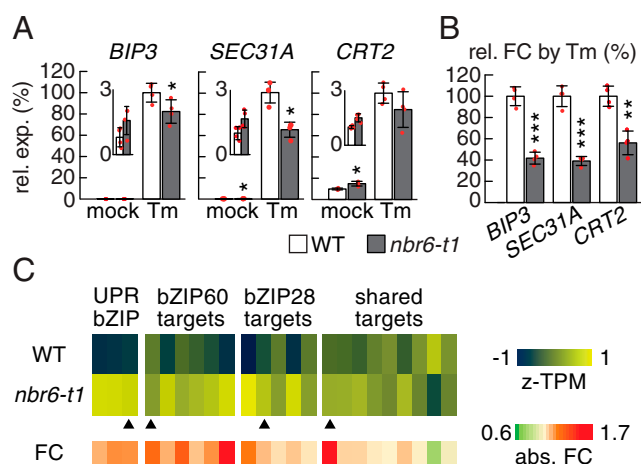


Fig. 6. UPR response of *nbr6-t1* single mutant to ER stress. (A and B) Relative expression levels of representative UPR genes in roots grown under ER-stress conditions (A) and their relative FC, with WT values set to 100% (B). Data are shown with all data points (red circles) and as bar graphs showing the average \pm SD from six biological replicates. Asterisks indicate significant difference relative to WT in the same group (Welch's *t* test, * $P < 0.05$; ** $P < 0.01$; *** $P < 0.001$). (C) UPR bZIPs and expression of their target genes in roots, as determined by RNA-seq analysis. Heatmaps illustrating z-standardized expression values (z-TPM; transcripts per million) and absolute FC values (abs. FC) in the *nbr6-t1* mutant. Black arrowheads starting from the left indicate values of *bZIP60*, *SEC31A*, *CRT2*, and *BIP3*.

In conclusion, the *nbr6-1* single mutant moderately induced UPR globally, likely explaining its shorter root under control conditions (Figs. 5A and 6C). Overall, the genotypes WT, *bz1728*, *bz1728nobiro6*, and *nbr6-1* exhibit varied UPR activity levels and varied primary root growth in an inversely associated relationship (SI Appendix, Fig. S5).

Discussion

Trade-offs between plant defense and growth are now widely accepted concepts (34, 35), whereas growth trade-offs in response to other stress categories are seldom considered. In this study, we discovered an inverse association between plant UPR activity and primary root growth (SI Appendix, Fig. S5). Using chemical agents and genetic manipulation, we observed that an increase in UPR is accompanied by a shortening of primary root growth (Figs. 1 and 5). In particular, the *nobiro6* suppressor mutant alleviated the overly activated UPR and the limited primary root growth of the *bz1728* double mutant (Figs. 3 and 4). The identification of *nobiro6* as loss-of-function allele of the TFIID component TAF12b indicated that transcriptome reprogramming is likely to provide a key to understanding the root growth defect by *bz1728*. As plant UPR responds to a broad spectrum of both biotic and abiotic stimuli (1, 4), and as the *bz1728* short root is due to composite defects of multiple root growth determinants (Figs. 1 and 3), we propose that the plant UPR acts as a key node between trade-offs, by integrating multiple stressful signals into a single regulatory module to control root growth as a function of the sum of all intracellular stress. Given that ethylene and cytokinin modulate both root growth and development (36, 37), the UPR may integrate these two phytohormone signaling pathways with NBR6/TAF12b at their crossroads (SI Appendix, Fig. S5). Future studies aimed at identifying other *nobiro* mutants will provide more players to integrate phytohormone homeostasis, stress signaling, and cell growth control in a model at the center of ER stress and UPR.

The transcriptome upheaval observed in the *bz1728* double mutant (Fig. 4A) masked whether the mutant short root was due to a defect in a growth-promoting signal or an excessive growth-limiting stress signal. The discovery and characterization of *nobiro6* answered this question, insofar as the induction of so many genes in *bz1728* is likely to be highly detrimental to root growth (Figs. 3 and 6). This hypothesis is also supported by the observation that many up-regulated genes in *bz1728* are stress-responsive (11). We note that the rescue of root growth by *nobiro6* was partial, and the UPR downstream genes responsible for the root growth defect are still unknown. The bZIP60 regulon is a possible candidate, although the overexpression of *bZIP60* did not affect root growth (38). However, the triple mutant of three UPR-bZIPs is embryo-lethal (11), and the *ire1a ire1b* double mutant lacking activity for the bZIP60 activators had modest but significant root growth defects that were enhanced when it was combined with *bzip17* in the *ire1a ire1b bzip17* triple mutant (13). These results indicate that the short root phenotype of the *bz1728* double mutant and the associated transcriptome turmoil are induced by multiple redundantly functioning ER stress-responsive transcription modulators, including bZIP60, and that NBR6 is a shared cofactor for their full activity.

We demonstrated that NBR6 functions as a transcriptional cofactor of the bZIP60 regulon, which requires physical interaction between bZIP60 and the C-terminal HFD of NBR6 (Fig. 4). In parallel, another transcriptional cofactor was reported for UPR, the nuclear factor Y (NF-Y) trimeric complex. A previous study found that a specific NF-Y complex physically interacts with bZIP28 through its HFD and assists the target promoter recognition, which are analogous to that of mammalian UPR-TF ATF6 (39). Given that NF-Y complex also interacts with TFIID

(40), these suggest how plant UPR-bZIPs form dimers to each other (11, 39) and how they are incorporated into the regulation of UPR downstream genes with other global TFs.

In contrast to TAF12b, no role has been reported for its ortholog TAF12a. Considering that TAF12 is typically encoded by a single and essential gene in yeast and metazoans, the viability of the *nbr6-1* mutant and the absence of a clearly defined role for TAF12a suggest the functional differentiation of the two *Arabidopsis* TAF12 proteins. In yeast and metazoans, TAF12 is a shared component of TFIID and the PIC subcomplex Spt-Ada-Gcn5 acetyltransferase (SAGA). These two subcomplexes have different target promoter preferences and influence the transcription of different genes involved in house-keeping or stress responses (41). The two *Arabidopsis* TAF12 proteins were recently shown to exhibit different affinities toward TFIID and SAGA components (42). The fungal pathogen *Candida albicans* also boasts two copies of TAF12 that participate in the growth of this unicellular organism nonredundantly, with each one showing selective interaction with the TFIID or SAGA complexes (43). Therefore, plants may also exploit multiple TAF12 isoforms for different purposes based on their interacting PIC subcomplexes, which may improve transcriptome plasticity and contribute to the strong environmental adaptability of plants.

Materials and Methods

Plant Materials and Growth Conditions. *A. thaliana* accession Columbia (Col-0) was used in this study. The T-DNA insertion lines (listed in SI Appendix, Table S3) were obtained from ABRC (Arabidopsis Biological Resource Center). The CRISPR/Cas9-mediated *nbr6-c1* mutant was induced with the pKAMA-ITACHI system (44). Transgenic *bz1728* lines expressing *NahG* were generated by *Agrobacterium*-mediated plant transformation as described previously (45). Detailed procedures for vector plasmid construction and transgenic plant generation are described in SI Appendix, Supplementary Materials and Methods. Seeds were surface-sterilized and stratified at 4 °C for 3 d in the dark before being sown onto the modified germination agar medium or on soil (11). Plants were grown in a growth chamber with a 16-h light/8-h dark photoperiod with fluorescent lights at $80 \pm 10 \mu\text{mol m}^{-2} \text{s}^{-1}$, 22 °C and 65% relative humidity.

Root Microscopy Imaging. Roots from 7-d-old *Arabidopsis* seedlings were stained with 10 mg L^{-1} propidium iodide (Thermo Fisher Scientific). The imaging data were obtained using a Leica SP5 confocal laser scanning microscope with a HC PL APO 20 \times 0.7 dry objective and a 488-nm argon-ion laser, or an Olympus FV1200 microscope with a UPlanSApo 20 \times 0.75 dry objective and a 559-nm LD laser line. The obtained images were exported with the software LAS X (version 3.7.2.22383; Leica) or FV10-ASW (version 04.02; Olympus). For cell length assays, each cell length was manually measured using ImageJ (v1.53g) (46).

Micrografting. Root-shoot grafting of 3-d-old seedlings was performed as described previously (47). The grafted seedlings were grown vertically for other 7 d, and then each seedling was photographed and the primary root growth was measured manually using ImageJ.

EMS Mutagenesis. Details of the procedure followed a previous report (48). In brief, 0.5 g of *bz1728* seeds were treated with 0.4% (vol/vol) EMS (M0880, Sigma-Aldrich) for 8 h at room temperature. After six washes with distilled water, the M₁ seeds were immediately sown on soil and grown in the growth conditions described above. The harvested M₂ seeds were vertically grown on the modified germination agar medium for 12 d, and the seedlings with longer roots than their neighbors were rescued for further validation of the phenotype in later generations.

Genome Resequencing. A total of 1 μg of *Arabidopsis* genomic DNA for each sample was subjected to DNA library construction for the Ion Proton system (Thermo Fisher Scientific) with the NEBNext Fast DNA library prep set (E6270, New England Biolabs). The sequencing resulted in an average of 6.2 million reads (151 nt in length on average) for each library. Read mapping and genetic variant calling were conducted as described in a previous report (45). Only biallelic single-nucleotide polymorphisms supported by more than five reads were retained for analysis.

RNA Extraction, cDNA Synthesis, and qRT-PCR. Total RNA was extracted with an RNeasy plant mini kit (Qiagen) and RNase-free DNase set (Qiagen). First-strand cDNA synthesis was conducted using the SuperScript VILO cDNA synthesis kit (Invitrogen). qPCR was performed on a 7500 Fast Real-Time PCR system and 7500 software (v2.0.6; Applied Biosystems). Fast SYBR Green master mix (Applied Biosystems) was used for amplification. *Arabidopsis ACTIN2* was used as reference gene. Primer sequences used for qPCR are given in *SI Appendix, Table S4*.

RNA-Seq. *Arabidopsis* samples were collected as four biological replicates. The roots from six 12-d-old seedlings were pooled as one replicate. Library construction for Illumina sequencing used the NEBNext Ultra II RNA library prep kit (E7770, New England Biolabs). Paired-end sequencing was performed on an Illumina HiSeq instrument, resulting in an average of 21.4 million reads (2 × 151 nucleotides) from each library. Clean reads were aligned to the *Arabidopsis* reference genome from Araport11 (49) with a Kallisto-Sleuth pipeline (v0.44.0) (50) for identifying DEGs. Detailed procedures are described in *SI Appendix, Supplementary Materials and Methods*.

Transient Expression Assays with *Arabidopsis* Mesophyll Protoplasts. Isolation and transformation procedures of *Arabidopsis* mesophyll protoplasts, as well as microscopy imaging, were conducted as described previously (11). The pGK-sGFP vector (45) was employed to determine the subcellular localization and transactivity of NBR6 derivatives. The pUC-VYCE(R) and pUC-VYNE(R) vectors were employed for BiFC analysis (27). Dual-luciferase reporter assays were performed to assess NBR6 transactivity. The pGK-ELUC vector (45) was used to drive expression of the emerald firefly luciferase reporter gene (*eLUC*) by the *BIP3* promoter. Cauliflower mosaic virus (CaMV) 35S promoter-driven *Renilla* luciferase (*hRLuc*) was used as internal control. LUC and RLUC activities were measured with reagents from a Dual-Luciferase Reporter Assay System (E1910, Promega) on an EnSpire Multimode Plate Reader and EnSpire Workstation software (v4.13.3005.1482; Perkin-Elmer). Detailed procedures for vector plasmid construction are described in *SI Appendix, Supplementary Materials and Methods*.

Split-Luciferase Assays. *Agrobacterium*-mediated transient infiltration in *N. benthamiana* leaves was conducted as previously reported (29) with minor adaptations. Leaf discs 7 mm in diameter cut from infiltrated leaves were applied to measure the LUC activity by EnSpire Multimode Plate Reader (Perkin-Elmer).

Chemical Treatments. Vertically grown 2-d-old *Arabidopsis* seedlings were transferred to new agar growth medium containing various concentrations of Tm (T7765; Sigma-Aldrich) or DTT (D1071; Tokyo Chemical Industry). The same

volume of dimethyl sulfoxide (DMSO) was used as mock control. The seedlings were grown vertically for other 7 d, then primary roots were photographed and their growth was measured manually using ImageJ.

Pull-Down Assays, SDS/PAGE, and Immunoblots. Tag-fused protein production and purification was achieved by employing the pCold system (TaKaRa Bio) and *E. coli* Rosetta(DE3) strain (Merck) according to the manufacturer's instructions. Detailed procedures for vector plasmid construction are described in *SI Appendix, Supplementary Materials and Methods*. The GST-tagged protein was extracted from cell pellets and purified on glutathione Sepharose 4B (GE Healthcare Life Sciences) beads, constituting the bait sample for pull-down assays. A total cell lysate obtained from *E. coli* cells producing the MBP-tagged protein was mixed with the loaded glutathione beads. The pull-down assay was carried out with Pierce GST protein interaction pull-down kit (Thermo Scientific). The resulting pulled-down proteins were run on 10% Bis-Tris NuPAGE Novex gel with MES running buffer (Thermo Scientific), after which proteins were transferred to a 0.2- μ m nitrocellulose membrane with the Transblot Turbo transfer system (Bio-Rad) and then subjected to immunoblot and chemiluminescent signal detection with the iBlot Western blot system (Thermo Scientific), ECL Prime detection reagent (Thermo Scientific), and ChemiDoc MP basic imaging system (Bio-Rad). Anti-GST (ab3416, Abcam; dilution 1:5,000), anti-MBP (E8032, New England Biolabs; dilution 1:10,000) and anti-mouse IgG (W4021, Promega; dilution 1:2,500) antibodies were used for immunoblotting.

Statistical Analyses. Welch's *t* test and one-way ANOVA post hoc Tukey's honestly significant difference (HSD) test were applied for two-sample and greater than two-sample comparisons, respectively.

Data Availability. The raw sequence data of *Arabidopsis* genome sequencing and RNA-seq were deposited at the National Center for Biotechnological Information Sequence Read Archive (BioProject IDs [PRJNA688172](https://www.ncbi.nlm.nih.gov/bioproject/PRJNA688172) and [PRJNA687636](https://www.ncbi.nlm.nih.gov/bioproject/PRJNA687636)). In-house scripts used in this study are available via the GitHub repository at <https://github.com/junesk9/>. All other study data are included in the article and/or supporting information.

ACKNOWLEDGMENTS. We thank Fuyuko Shimoda, Manami Masuda, and Saho Mizukado (RIKEN) for providing skillful technical assistance; and Taiji Kawakatsu (National Agriculture & Food Research Organization, Japan) for providing excellent technical support for the transcriptome analysis. This work was supported by Grants-in-Aid for Scientific Research (C) (21K05524) from the Japan Society for the Promotion of Science, by Inamori Research Grants from the Inamori Foundation, and by a grant from the Special Postdoctoral Researcher program from RIKEN (to J.-S.K.).

1. S. H. Howell, Endoplasmic reticulum stress responses in plants. *Annu. Rev. Plant Biol.* **64**, 477–499 (2013).
2. C. Hetz, K. Zhang, R. J. Kaufman, Mechanisms, regulation and functions of the unfolded protein response. *Nat. Rev. Mol. Cell Biol.* **21**, 421–438 (2020).
3. F. Brandizzi, Maintaining the structural and functional homeostasis of the plant endoplasmic reticulum. *Dev. Cell* **56**, 919–932 (2021).
4. E. Angelos, C. Ruberti, S.-J. Kim, F. Brandizzi, Maintaining the factory: The roles of the unfolded protein response in cellular homeostasis in plants. *Plant J.* **90**, 671–682 (2017).
5. J.-X. Liu, R. Srivastava, P. Che, S. H. Howell, Salt stress responses in *Arabidopsis* utilize a signal transduction pathway related to endoplasmic reticulum stress signaling. *Plant J.* **51**, 897–909 (2007).
6. J.-X. Liu, R. Srivastava, P. Che, S. H. Howell, An endoplasmic reticulum stress response in *Arabidopsis* is mediated by proteolytic processing and nuclear relocation of a membrane-associated transcription factor, bZIP28. *Plant Cell* **19**, 4111–4119 (2007).
7. H. Gao, F. Brandizzi, C. Benning, R. M. Larkin, A membrane-tethered transcription factor defines a branch of the heat stress response in *Arabidopsis thaliana*. *Proc. Natl. Acad. Sci. U.S.A.* **105**, 16398–16403 (2008).
8. Y. Iwata *et al.*, Activation of the *Arabidopsis* membrane-bound transcription factor bZIP28 is mediated by site-2 protease, but not site-1 protease. *Plant J.* **91**, 408–415 (2017).
9. Y. Deng *et al.*, Heat induces the splicing by IRE1 of a mRNA encoding a transcription factor involved in the unfolded protein response in *Arabidopsis*. *Proc. Natl. Acad. Sci. U.S.A.* **108**, 7247–7252 (2011).
10. Y. Nagashima *et al.*, *Arabidopsis* IRE1 catalyses unconventional splicing of bZIP60 mRNA to produce the active transcription factor. *Sci. Rep.* **1**, 29 (2011).
11. J.-S. Kim, K. Yamaguchi-Shinozaki, K. Shinozaki, ER-anchored transcription factors bZIP17 and bZIP28 regulate root elongation. *Plant Physiol.* **176**, 2221–2230 (2018).
12. P. Che *et al.*, Signaling from the endoplasmic reticulum activates brassinosteroid signaling and promotes acclimation to stress in *Arabidopsis*. *Sci. Signal.* **3**, ra69–ra69 (2010).
13. Y. Bao, D. C. Bassham, S. H. Howell, A functional unfolded protein response is required for normal vegetative development. *Plant Physiol.* **179**, 1834–1843 (2019).
14. Y. Xu *et al.*, A TFIIID-SAGA perturbation that targets MYB and suppresses acute myeloid leukemia. *Cancer Cell* **33**, 13–28.e8 (2018).
15. P.-J. Hamard *et al.*, A functional interaction between ATF7 and TAF12 that is modulated by TAF4. *Oncogene* **24**, 3472–3483 (2005).
16. S. Hintze, M. Engelhardt, L. van Diepen, E. Witt, H.-J. Schüller, Multiple Taf subunits of TFIIID interact with Ino2 activation domains and contribute to expression of genes required for yeast phospholipid biosynthesis. *Mol. Microbiol.* **106**, 876–890 (2017).
17. K. A. Garbett, M. K. Tripathi, B. Cencki, J. H. Layer, P. A. Weil, Yeast TFIIID serves as a coactivator for Rap1p by direct protein-protein interaction. *Mol. Cell. Biol.* **27**, 297–311 (2007).
18. L. M. Robles, J. S. Wampole, M. J. Christians, P. B. Larsen, *Arabidopsis* enhanced ethylene response 4 encodes an EIN3-interacting TFIIID transcription factor required for proper ethylene response, including ERF1 induction. *J. Exp. Bot.* **58**, 2627–2639 (2007).
19. M. Kubo, T. Kakimoto, The cytokinin-hypersensitive genes of *Arabidopsis* negatively regulate the cytokinin-signaling pathway for cell division and chloroplast development. *Plant J.* **23**, 385–394 (2000).
20. M. Kubo *et al.*, The CKH1/EEER4 gene encoding a TAF12-like protein negatively regulates cytokinin sensitivity in *Arabidopsis thaliana*. *Plant Cell Physiol.* **52**, 629–637 (2011).
21. H. Jin, Z. Yan, K. H. Nam, J. Li, Allele-specific suppression of a defective brassinosteroid receptor reveals a physiological role of UGGT in ER quality control. *Mol. Cell* **26**, 821–830 (2007).
22. H. Jin, Z. Hong, W. Su, J. Li, A plant-specific calreticulin is a key retention factor for a defective brassinosteroid receptor in the endoplasmic reticulum. *Proc. Natl. Acad. Sci. U.S.A.* **106**, 13612–13617 (2009).
23. Y. Liu *et al.*, EB57 is a plant-specific component of a highly conserved endoplasmic reticulum-associated degradation system in *Arabidopsis*. *Proc. Natl. Acad. Sci. U.S.A.* **112**, 12205–12210 (2015).
24. T. P. Delaney, L. Friedrich, J. A. Ryals, *Arabidopsis* signal transduction mutant defective in chemically and biologically induced disease resistance. *Proc. Natl. Acad. Sci. U.S.A.* **92**, 6602–6606 (1995).

25. C. Gaillochet *et al.*, HY5 and phytochrome activity modulate shoot-to-root coordination during thermomorphogenesis in *Arabidopsis*. *Development* **147**, dev192625 (2020).
26. G. M. Nawkar *et al.*, HY5, a positive regulator of light signaling, negatively controls the unfolded protein response in *Arabidopsis*. *Proc. Natl. Acad. Sci. U.S.A.* **114**, 2084–2089 (2017).
27. R. Waadt *et al.*, Multicolor bimolecular fluorescence complementation reveals simultaneous formation of alternative CBL/CIPK complexes in planta. *Plant J.* **56**, 505–516 (2008).
28. Y. Iwata, N. V. Fedoroff, N. Koizumi, Arabidopsis bZIP60 is a proteolysis-activated transcription factor involved in the endoplasmic reticulum stress response. *Plant Cell* **20**, 3107–3121 (2008).
29. H. Chen *et al.*, Firefly luciferase complementation imaging assay for protein-protein interactions in plants. *Plant Physiol.* **146**, 368–376 (2008).
30. Y. Deng, R. Srivastava, S. H. Howell, Protein kinase and ribonuclease domains of IRE1 confer stress tolerance, vegetative growth, and reproductive development in *Arabidopsis*. *Proc. Natl. Acad. Sci. U.S.A.* **110**, 19633–19638 (2013).
31. C. Ruberti, Y. Lai, F. Brandizzi, Recovery from temporary endoplasmic reticulum stress in plants relies on the tissue-specific and largely independent roles of bZIP28 and bZIP60, as well as an antagonizing function of BAX-Inhibitor 1 upon the pro-adaptive signaling mediated by bZIP28. *Plant J.* **93**, 155–165 (2018).
32. Y. Iwata, N. Koizumi, An Arabidopsis transcription factor, AtbZIP60, regulates the endoplasmic reticulum stress response in a manner unique to plants. *Proc. Natl. Acad. Sci. U.S.A.* **102**, 5280–5285 (2005).
33. Y. Deng *et al.*, IRE1, a component of the unfolded protein response signaling pathway, protects pollen development in *Arabidopsis* from heat stress. *Plant J.* **88**, 193–204 (2016).
34. E. Smakowska, J. Kong, W. Busch, Y. Belkadir, Organ-specific regulation of growth-defense tradeoffs by plants. *Curr. Opin. Plant Biol.* **29**, 129–137 (2016).
35. B. Huot, J. Yao, B. L. Montgomery, S. Y. He, Growth-defense tradeoffs in plants: A balancing act to optimize fitness. *Mol. Plant* **7**, 1267–1287 (2014).
36. I. I. Vaseva *et al.*, The plant hormone ethylene restricts *Arabidopsis* growth via the epidermis. *Proc. Natl. Acad. Sci. U.S.A.* **115**, E4130–E4139 (2018).
37. C. Artner, E. Benkova, Ethylene and cytokinin—Partners in root growth regulation. *Mol. Plant* **12**, 1312–1314 (2019).
38. S. Humbert, S. Zhong, Y. Deng, S. H. Howell, S. J. Rothstein, Alteration of the bZIP60/IRE1 pathway affects plant response to ER stress in *Arabidopsis thaliana*. *PLoS One* **7**, e39023 (2012).
39. J.-X. Liu, S. H. Howell, bZIP28 and NF-Y transcription factors are activated by ER stress and assemble into a transcriptional complex to regulate stress response genes in *Arabidopsis*. *Plant Cell* **22**, 782–796 (2010).
40. M. Frontini *et al.*, NF-Y recruitment of TFIID, multiple interactions with histone fold TAF(II)s. *J. Biol. Chem.* **277**, 5841–5848 (2002).
41. S. V. Antonova, J. Boeren, H. T. M. Timmers, B. Snel, Epigenetics and transcription regulation during eukaryotic diversification: The saga of TFIID. *Genes Dev.* **33**, 888–902 (2019).
42. C.-J. Wu *et al.*, Three functionally redundant plant-specific paralogs are core subunits of the SAGA histone acetyltransferase complex in *Arabidopsis*. *Mol. Plant* **14**, 1071–1087 (2021).
43. I. Sinha, S. Kumar, P. Poonia, S. Sawhney, K. Natarajan, Functional specialization of two paralogous TAF12 variants by their selective association with SAGA and TFIID transcriptional regulatory complexes. *J. Biol. Chem.* **292**, 6047–6055 (2017).
44. H. Tsutsui, T. Higashiyama, pKAMA-ITACHI vectors for highly efficient CRISPR/Cas9-mediated gene knockout in *Arabidopsis thaliana*. *Plant Cell Physiol.* **58**, 46–56 (2017).
45. S. Kidokoro *et al.*, *DREB1A/CBF3* is repressed by transgene-induced DNA methylation in the *Arabidopsis ice1-1* mutant. *Plant Cell* **32**, 1035–1048 (2020).
46. C. A. Schneider, W. S. Rasband, K. W. Eliceiri, NIH Image to ImageJ: 25 years of image analysis. *Nat. Methods* **9**, 671–675 (2012).
47. F. Takahashi *et al.*, A small peptide modulates stomatal control via abscisic acid in long-distance signalling. *Nature* **556**, 235–238 (2018).
48. Y. Kim, K. S. Schumaker, J.-K. Zhu, EMS mutagenesis of *Arabidopsis*. *Methods Mol. Biol.* **323**, 101–103 (2006).
49. C.-Y. Cheng *et al.*, Araport11: A complete reannotation of the *Arabidopsis thaliana* reference genome. *Plant J.* **89**, 789–804 (2017).
50. H. Pimentel, N. L. Bray, S. Puente, P. Melsted, L. Pachter, Differential analysis of RNA-seq incorporating quantification uncertainty. *Nat. Methods* **14**, 687–690 (2017).